Damping and spin mixing conductance in $Ni_{80}Fe_{20}$/CuIr structures: effect of Ir doping

2017 J. Phys. D: Appl. Phys. 50 135002

(http://iopscience.iop.org/0022-3727/50/13/135002)

IOP Publishing Journal of Physics D: Applied Physics
J. Phys. D: Appl. Phys. **50** (2017) 135002 (7pp) https://doi.org/10.1088/1361-6463/aa5b63

Damping and spin mixing conductance in $Ni_{80}Fe_{20}$/CuIr structures: effect of Ir doping

M Belmeguenai[1], M S Gabor[2], F Zighem[1] and C Tiusan[2,3]

[1] LSPM-CNRS, Université Paris XIII-Sorbonne Paris Cité, 93430 Villetaneuse, France
[2] Center for Superconductivity, Spintronics and Surface Science, Technical University of Cluj-Napoca, Str. Memorandumului No. 28 RO-400114, Cluj-Napoca, Romania
[3] Institut Jean Lamour, CNRS, Université de Nancy, BP 70239, F–54506 Vandoeuvre, France

E-mail: belmeguenai.mohamed@univ-paris13.fr and mihai.gabor@phys.utcluj.ro

Received 13 September 2016, revised 10 November 2016
Accepted for publication 23 January 2017
Published 27 February 2017

Abstract

$Ni_{80}Fe_{20}$(Py) thin films of different thicknesses have been sputtered on thermally oxidized Si substrates and capped with Pt or Cu doped with 6%, 3% and 1% of Ir. Vibrating sample magnetometery has been used to measure the magnetization at saturation. Microstrip line ferromagnetic resonance (MS-FMR) has been used to investigate the Py and capping layer thickness dependence of the damping parameter enhancement due to the spin pumping. The experimental data have been analyzed using a model for spin pumping that includes the effective spin mixing conductance at the Py/HM (HM = Pt and CuIr) interface and the spin-diffusion length of HM. The spin mixing conductance (spin diffusion length) increases (decreases) as Ir doping increases. For samples capped with Pt (CuIr(6%)), the obtained values of spin mixing conductance and the spin diffusion length have been estimated to be 25 nm^{-2} (9.87 nm^{-2}) and 1.05 nm (2.8 nm), respectively. MS-FMR measurements revealed that the effective magnetization varies linearly with the effective Py thickness due to the perpendicular surface anisotropy.

Keywords: spin pumping, ferromagnetic resonance, Gilbert damping, spin Hall effect, spin mixing conductance

(Some figures may appear in colour only in the online journal)

1. Introduction

Generation, manipulation and detection of the spin current (the flow of angular momentum) in spintronics devices are of high importance and necessary for the realization of efficient spin-based magnetic memories and logic devices [1]. The spin current can be generated in different ways: by spin injection from a ferromagnetic material [2, 3], by spin Hall effect (SHE) [4–7] (spin up and spin down transverse accumulation on opposite sides of a current-carrying conductor due to spin–orbit coupling (SOC)), by spin Seebeck effect [8] or by spin pumping [9, 10]. In the latter method, the precession of the magnetization of the ferromagnetic layer (FM) induces a pure spin current that can be detected as a voltage drop in a juxtaposed nonmagnetic metallic layer (NM) via the inverse spin Hall effect (ISHE) [11–13] again through SOC. The origin of the SHE and ISHE can be intrinsic, as in the case of materials with high atomic number such as Pt (the most commonly used), for which SOC is embedded in the electronic structure, or extrinsic, due to asymmetric spin-dependent scatterings on impurities with large SOC [14, 15], as in the case of Cu doped with Ir (CuIr) [16].

The relevant property that characterizes the ability of the spin current to pass through the FM-NM interface and its relaxation in the NM is the effective spin mixing conductance $g_{\mathrm{eff}}^{\uparrow\downarrow}$. This parameter is affected by the existence of strong spin–orbit coupling if the metal layer (NM) is a heavy metal (HM). Indeed, the spins are pumped into the HM layer where the spin of the electron can either relax by spin-flip scattering due to the SOC or flows back into the ferromagnet. Therefore the interface determines the spin current resulting in the HM layer. The spin current then exerts an additional torque on the magnetization, thus increasing the Gilbert damping parameter α of FM/NM heterostructures. The Gilbert damping parameter,

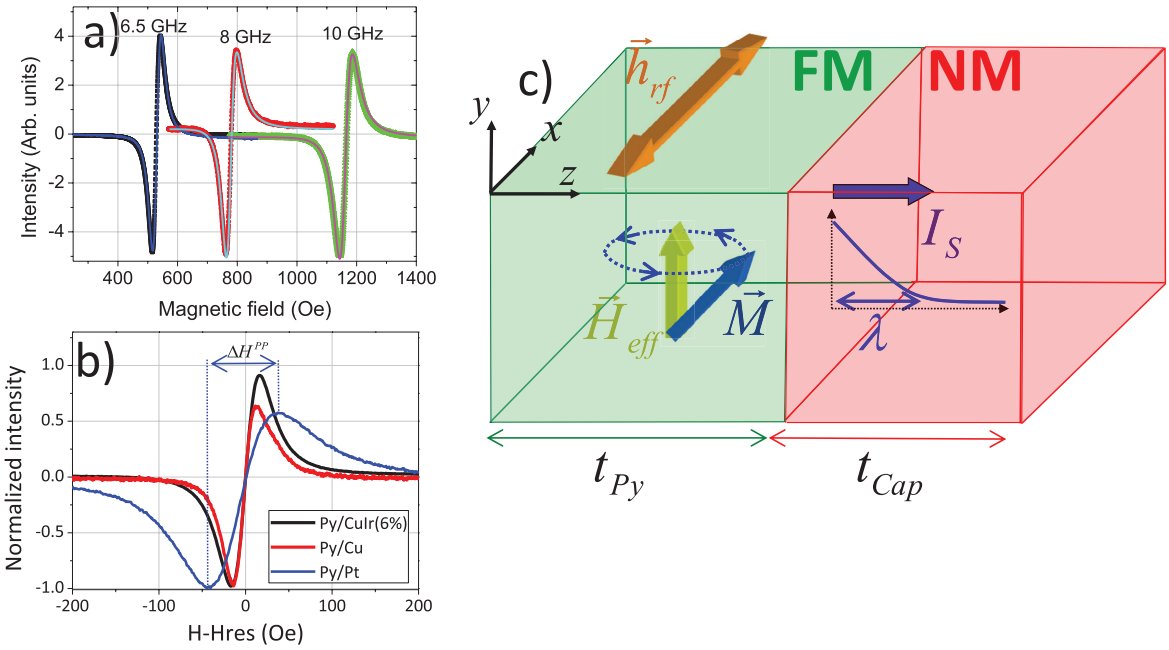

Figure 1. (a) Ferromagnetic resonance spectra representing the amplitude of the field derivative of the absorption as a function of the applied magnetic field for 6 nm thick Py layer capped with 8 nm thick CuIr(6%), measured at different driven frequencies. Symbols refer to experimental data and solid lines are fits by Lorentzian derivative. (b) Ferromagnetic resonance spectra representing the normalized amplitude of the field derivative of the absorption as a function of the applied magnetic field for 4 nm thick Py layers capped with Pt, CuIr(6%) and Cu. For direct comparison of the linewidth, the spectra have been horizontaly shifted by their respective resonance fields. Due the spin pumping, the enhancement of the linewidth depends on the capping layer. (c) Representation of the spin pumping effect at the interface FM/NM: the resonant precession of the magnetization pumps a spin current I_S into NM. This generated spin current diffuses into the NM layer and dissipates within the spin diffusion length λ. The relaxation of I_S in the nonmagnetic layer corresponds to a loss of angular momentum in the ferromagnetic layer and results in an increase of the effective Gilbert damping.

which expresses the dissipation of magnetic energy and hence relaxation of magnetization is a key factor for determining the performance of magnetic materials in a multitude of applications. Indeed, it is an important parameter in spintronics, since the critical current density of the spin transfer torque current-induced magnetization [17] reversal is proportional to α [18], while short switching time magnetization reversal is achieved for a large α [19]. Therefore, precise experimental determination and control of α are needed.

The purpose of this study is to use the ferromagnetic resonance to determine the variation of the Gilbert damping parameter as a function of the thicknesses of $Ni_{80}Fe_{20}$ and HM layers in heterostructures of $Ni_{80}Fe_{20}$ /HM (where HM = Pt and Cu doped by 1%, 3% and 6% of Ir). We show that α increases linearly with the inverse of $Ni_{80}Fe_{20}$ effective thickness allowing to determine the effective spin mixing conductance, which is found to increase with the increasing Ir doping rate. The Pt and CuIr thickness dependence of α has been used to determine the spin diffusion length, which is found to increase with decreasing Ir doping rates and significantly lower in the case of Pt.

2. Samples and experimental techniques

Two sets of samples, consisting of Pt and $Ni_{80}Fe_{20}$ (Py) or $Ni_{80}Fe_{20}$ and Cu doped with CuIr(x%), where $x = 1$, 2 and 3, stacks grown onto Si/SiO_2 substrates have been used in this study. For this, Py layers with variable thickness (2 nm $\leqslant t_{Py} \leqslant$ 10 nm) were deposited at room temperature onto a Si substrate covered with a 100 nm thick thermally oxidized SiO_2 layer using a magnetron sputtering system. The Py layers were then *in situ* capped by Pt layer (1 nm $\leqslant t_{Pt} \leqslant$ 12 nm) or by a bilayer of CuIr (x%)/Al(2 nm). The thickness of the CuIr has been varied from 1 to 16 nm (1 nm $\leqslant t_{CuIr} \leqslant$ 16 nm). In these heterostructures, the Pt and CuIr are used as HM layers and Al is used as a passivation layer to avoid the oxidation of CuIr. Samples with varying Py or HM thicknesses are used to determine the spin mixing conductance or the spin diffusion length via the thickness dependence of the Gilbert damping parameter of FM/NM heterostructures. In order to study the dependence of the gyromagnetic factor on the capping layer thickness, 3.5 nm thick Py films capped with a 5 nm thick Cu or Ta layer have also been grown in similar conditions.

All experiments have been performed at room temperature. Vibrating sample magnetometery (VSM) has been used to measure the hysteresis loops of the samples with a magnetic field applied in the sample plane and to determine the magnetization at saturation M_s. Microstrip line ferromagnetic resonance (MS-FMR) [20], which is a versatile and widely used technique, has been employed here for studying the magnetic anisotropy and the relaxation in our films. In MS-FMR experiment, the magnetic sample is mounted on a microstrip line (composed of 0.5 mm Cu strip grown on Cu-back side metalized Al_2O_3 substrate, designed to have 50Ω characteristic

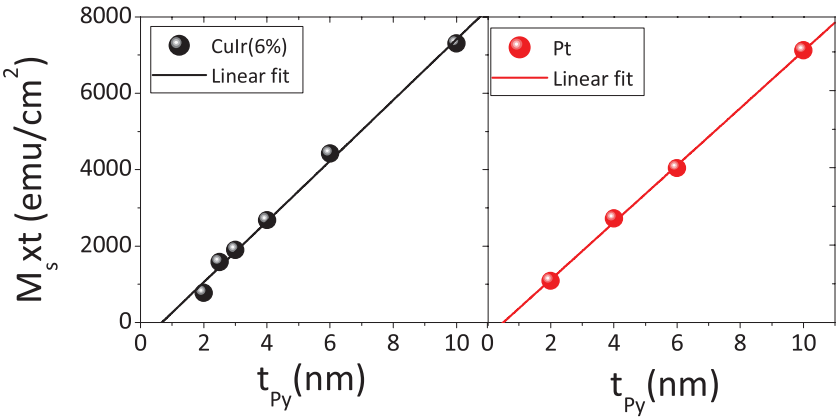

Figure 2. Thickness dependences of the saturation magnetic moment per unit area for Py thin films grown on Si substrates and capped with Pt and Cu doped with 6% of Ir (CuIr(6%)). Symbols refer to measurements and solid lines are the linear fits.

impedance and broadband), which is connected to a Hewlett-Packard network analyzer (N5230A), operating in the range 0.01–40 GHz, and to a Schottky detector used to measure the transmitted power. For each driven frequency, the sample is swept through the resonance by varying the applied external field (up to 1.9 T). In addition, the external magnetic field is modulated at 170 Hz by small (4 Oe) alternating magnetic field allowing lock-in detection via a lock-in amplifier (Stanford research system SR830). The recorded signal is thus proportional to the field derivative of the imaginary part of the rf susceptibility as a function of the applied magnetic field. The resonance field and the peak to peak FMR linewidth are obtained from a fit assuming a Lorentzian derivative shape of the recorded data (as shown on figure 1(a) for 6 nm thick Py film capped by a 8 nm thick CuIr(6%) layer). This broadband MS-FMR set-up offers a high sensitivity allowing detecting a net magnetic moment down to 10^{-5} emu. The magnetic anisotropy of the different samples is extracted from in-plane angular dependence of the uniform precession mode resonance field. The complete analysis of in-plane and perpendicular applied field spectra exhibiting uniform precession modes leads to the determination of most of the magnetic parameters: effective magnetization, gyromagnetic factor and anisotropy terms.

Figure 1(b), shows the FMR spectrum of 4 nm thick Py films capped with CuIr(6%), Pt or Cu layers, measured at 6 GHz driven frequency. The FMR linewidth of the Py/Pt is clearly greater than that of Py/CuIr(6%) and Py/Cu, which shows the narrower linewidth. Since the spectral width is proportional to the Gilbert damping constant α (as shown below), one can conclude that the enhancement of the damping constant is due to the magnetization precession relaxation mechanism, which is capping layer dependent. In fact, the resonant precession of the magnetization pumps a spin current I_S into NM as shown in figure 1(c). If the NM layer is a perfect spin sink, the generated spin current diffuses into the NM layer and dissipates within the spin diffusion length λ. The relaxation of the spin current in the nonmagnetic layer corresponds to a loss of angular momentum in the ferromagnetic layer and results in an increase in the effective Gilbert damping of the magnetization precession. Here, we use the angular dependences of the FMR linewidth in order to identify the direction of the applied field giving the minimum of the FMR linewidth corresponding to minimal extrinsic relaxation mechanisms responsible for the line broadening. The frequency dependence of the FMR linewidth is then measured for an applied field along this direction and the Gilbert damping parameter is thus deduced and studied as a function of the Py and HM thicknesses.

3. Theoretical background

The experimental dynamic data presented here have been analyzed considering the model described in [20]. According to this model and since the resonance fields in perpendicular applied magnetic field configuration are large (>5 kOe in our samples even at low frequencies), the small magnetic in-plane anisotropy fields of the studied samples can been neglected. Therefore, the resonance expression of the uniform precession mode assuming a perpendicular applied magnetic field is given by :

$$F_{\perp} = \left(\frac{\gamma}{2\pi}\right)(H - 4\pi M_{\text{eff}}). \tag{1}$$

For in-plane applied magnetic fields, the resonance expression of the uniform precession mode is given by :

$$F_{\parallel}^2 = \left(\frac{\gamma}{2\pi}\right)^2 \left[\left(H\cos(\varphi_M - \varphi_H) + \frac{2K_4}{M_s}\cos 4(\varphi_M - \varphi_4) + \frac{2K_u}{M_s}\cos 2(\varphi_M - \varphi_u)\right)\right.$$
$$\left.(H\cos(\varphi_M - \varphi_H) + 4\pi M_{\text{eff}} + \frac{K_4}{2M_s}(3 + \cos 4(\varphi_M - \varphi_4)) + \frac{K_u}{M_s}(1 + \cos 2(\varphi_M - \varphi_u))\right] \tag{2}$$

$\gamma/2\pi = g \times 1.397 \times 10^6$ Hz Oe^{-1} is the gyromagnetic factor.

In the above expressions, φ_M represent the in-plane (referring to the substrate edges) angle defining the direction of the magnetization M. φ_u and φ_4 define the angles between the planar uniaxial easy axis and the planar fourfold easy axis with respect to the substrate edges, respectively. K_u, K_4 and $K_\perp$ are the in-plane uniaxial, the fourfold and the out-of-plane uniaxial anisotropy constants, respectively. We introduce $H_u = \frac{2K_u}{M_s}$ and $H_4 = \frac{2K_4}{M_s}$ as the in-plane uniaxial and the fourfold anisotropy fields and we define the effective magnetization $M_{\rm eff} = H_{\rm eff}/4\pi$ obtained by:

$$4\pi M_{\rm eff} = 4\pi M_{\rm s} - \frac{2K_\perp}{M_{\rm s}}. \quad (3)$$

Note that, in this study, the effective perpendicular anisotropy term $K_\perp$ could be phenomenologically separated in a volume and interfaces contributions and approximately obeyed the relation:

$$K_\perp = K_{v\perp} + \frac{2K_{s\perp}}{t} \quad (4)$$

where $K_{s\perp}$ refers to the perpendicular anisotropy term of the interfacial energy density and $K_{v\perp}$ is the volume anisotropy constant.

In FMR experiments, the peak-to-peak FMR linewidth $\Delta H^{\rm PP}$ is directly related to the damping and consists of intrinsic and extrinsic contributions. The intrinsic contribution is not angular dependent (when the applied field and the magnetization are parallel); it derives from the Gilbert damping and is given by:

$$\Delta H^{\rm Gi} = \frac{2}{\sqrt{3}}\frac{\alpha}{\gamma}2\pi f \quad (5)$$

where f is the driven frequency and α is the Gilbert coefficient. The relevant mechanisms [21] describing the extrinsic contributions, which are angular dependent, are usually mosaicity (the orientation spread of the crystallites), inhomogeneity and two magnon scattering [22–24]. Due to its very weak in-plane angular dependence (as it will be shown below), the frequency dependence of $\Delta H^{\rm PP}$ in our samples has been expressed as:

$$\Delta H^{\rm PP} = \Delta H_0 + \frac{2}{\sqrt{3}}\frac{\alpha}{\gamma}2\pi f \quad (6)$$

ΔH_0 describes an inhomogeneous broadening term due to the sample imperfections and is assumed to be frequency and angle independent.

4. Results and discussion

For all the studied films, the hysteresis loops were measured by VSM with an in-plane applied magnetic fields. The thickness dependencies of the saturation magnetic moment per unit area, deduced from these hysteresis loops, are shown in figure 2. The thickness dependences of the magnetic moment are used to determine the magnetization at saturation (M_s) and the magnetic dead layer (t_d): the slope gives the saturation magnetization, while the horizontal axis intercept gives the extent of the magnetic dead layer. The thickness of the magnetic dead layer and magnetization at saturation are found to be 0.5 nm (0.6 nm) and 748 ± 20 emu cm^{-3} (795 ± 30 emu cm^{-3}) for the Pt (CuIr(6%)) capped films. The obtained values of M_s are very close and the small discrepancy is within the error bar.

The g value, which determines the gyromagnetic factor and therefore the precision of the evaluation of α, is precisely

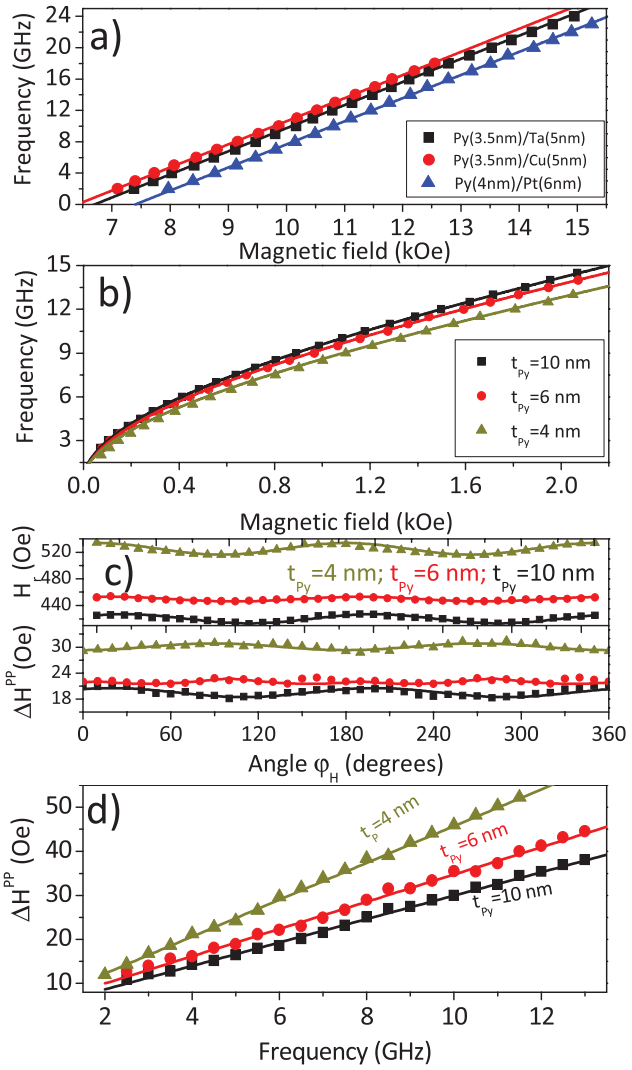

Figure 3. (a) Variation of the uniform precession mode frequency as a function of the perpendicular applied magnetic field for 3.5 and 4 nm thick Py films capped with Ta, Pt or CuIr(6%). (b) Easy axis field dependence of the resonance frequency of the uniform precession mode of Py thin films of thickness ($t_{\rm Py}$) capped with 8 nm thick CuIr(6%). (c) Angular dependencies of the resonance field (H_r) and peak-to-peak field FMR linewidth ($\Delta H^{\rm PP}$) measured at 6 GHz driving frequency for Py thin films of thickness ($t_{\rm Py}$) capped with 8 nm thick CuIr(6%) layer. Symbols refer to the experimental data and solid lines are the fits using equations (1) and (2) and the magnetic parameters indicated in the text. Solid lines for $\Delta H^{\rm PP}$ are used to guide the eyes. (d) Frequency dependences of the peak-to-peak field FMR linewidth ($\Delta H^{\rm PP}$) of Py thin films of thickness ($t_{\rm Py}$) capped with a 8 nm thick CuIr(6%). The magnetic field has been applied along the direction giving the minimal linewidth determined from the angular dependence of $\Delta H^{\rm PP}$. Symbols refer to the experimental data and solid lines are fits using equation (6) and the magnetic parameters indicated in text.

Table 1. Magnetic parameters obtained from the best fits to our experimental FMR results with the above mentioned model.

Cap layer	t_d (nm)	$K_{\perp s}$ (erg · cm^{-2})	$K_{\perp v}$ (erg · cm^{-3})	$g_{\text{eff}}^{\downarrow\uparrow}$ (nm^{-2})	$g_{\text{Cap}}^{\downarrow\uparrow}$ (nm^{-2})	α_{Py}	λ (nm)
Pt	0.5	0.36 ± 0.01	0.37×10^5	25 ± 1	24.8 ± 1	6.7×10^{-3}	1.05 ± 0.1
CuIr(6%)	0.6	0.37 ± 0.01	-1.39×10^5	9.87 ± 0.4	9.6 ± 0.4	5×10^{-3}	2.8 ± 0.2
CuIr(3%)	0.6	0.42 ± 0.015	-1.39×10^5	7.95 ± 0.3	8.07 ± 0.3	5.2×10^{-3}	3.4 ± 0.2
CuIr(1%)	0.6	0.43 ± 0.015	-1.39×10^5	5.9 ± 0.2	5.9 ± 0.2	5×10^{-3}	3.8 ± 0.2

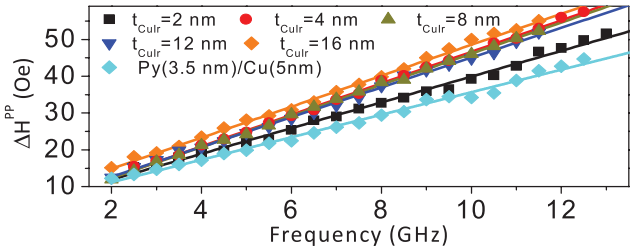

Figure 4. Frequency dependence of ΔH^{PP} for 4 nm thick Py thin films capped with CuIr(6%) layer of thickness (t_{CuIr}). For comparison, the frequency dependence of ΔH^{PP} for Py(3.5 nm) capped with a 5 nm thick Cu layer is also shown. The solid lines refer to the fit using the above mentioned models.

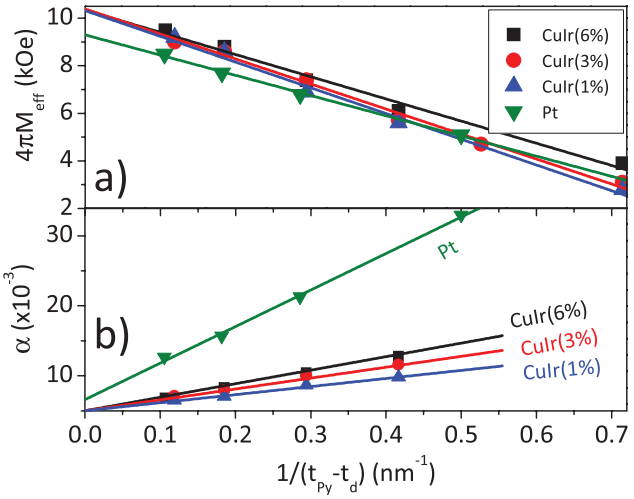

Figure 5. Thickness dependence of (a) the effective magnetization ($4\pi M_{\text{eff}}$) and (b) intrinsic damping parameter (α) extracted from the fit of FMR measurements of Py thin films of thickness (t_{Py}) capped with 8 nm thick CuIr(1%, 3% and 6%) and 6 nm thick Pt layers. The solid lines are the linear fits.

accessible by the MS-FMR technique using equation (1), through the study of the frequency variation versus the magnetic field applied perpendicularly to the film plane. The typical MS-FMR perpendicular field dependence of the resonance frequency for three Py films capped with Ta, Cu and Pt is shown in figure 3(a). Its linear variation as a function of the magnetic field is in excellent agreement with the calculated ones using equation (1) with $g = 2.109$ ($\gamma/2\pi = 29.5$ GHz T^{-1}). The derived value of g is in excellent agreement with the value determined in a recent paper [25] addressing the precise determination of the spectroscopic g factor in Py by broadband ferromagnetic resonance measurements. Moreover, this value does not present a significant variation versus the capping layer material and therefore, it will be used for all the samples studied here.

Figure 3(c) shows the typical angular dependence of the resonance field (at 6 GHz driven frequency) for different Py films capped with 8 nm thick CuIr(6%). The typical angular behavior is governed by a small uniaxial anisotropy contribution not exceeding 12 Oe. All the investigated samples in this study present a similar behavior except the 4 nm thick Py films capped with CuIr(6%) of a variable thickness, the 3 nm and 4 nm thick Py films capped with 8 nm thick CuIr(3%) layer, where small fourfold anisotropy superimposed to uniaxial term have been observed. Since, the primary goal of this paper is the spin pumping, the anistropy nature and origin and their thickness dependences will not be considered here. The corresponding field dependences of the uniform precession mode frequency recorded for the applied field along the easy axis of Py thin films capped with CuIr(6%) layer are shown on figure 3(b). By conjointly fitting the data in figures 3(b) and (c) to the above presented model, the effective magnetization ($4\pi M_{\text{eff}}$) and the anisotropy fields are extracted. Interestingly, the effective magnetization, shown on figure 5(a) for all the films capped with the different materials, follows a linear variation versus the inverse of the effective thickness of the Py ($1/(t_{\text{Py}} - t_{\text{d}})$). The linear fit of the measurements allows us to determine the value of the perpendicular surface anisotropy constants summarized in table 1. The $4\pi M_{\text{eff}}$ value when $t_{\text{Py}} - t_{\text{d}}$ tends to infinity, equal to 10.34 kOe and 9.3 kOe for CuIr and Pt respectively, is slightly different from the M_{s} values mentioned above, suggesting a small volume perpendicular anistropy.

In figure 3(c), the FMR peak-to-peak linewidth (ΔH^{PP}) is plotted as a function of the applied field angle φ_H for the CuIr capped Py films of various thicknesses using 6 GHz driving frequency. ΔH^{PP} is defined as the field difference between the extrema of the FMR derivative curve. All the other samples show a qualitatively similar behavior to one of the samples presented here. The positions of the extrema depend on the sample. The observed small anisotropy of the linewidth cannot be due to the Gilbert damping contribution, which is expected to be isotropic, and must be due to an additional extrinsic damping mechanism. Due to the very weak angular dependence of the linewidth and since the primary goal of this paper is the investigation of the spin diffusion length and the spin mixing conductance, the identification of the extrinsic relaxation mechanisms and their variations as a function of FM and HM thicknesses are not considered here. Therefore, this angular dependence for each sample is used to determine the applied field direction giving the minimum of the linewidth ΔH^{PP}, for which the frequency dependence of ΔH^{PP} is then measured for the sake of the minimization of the extrinsic

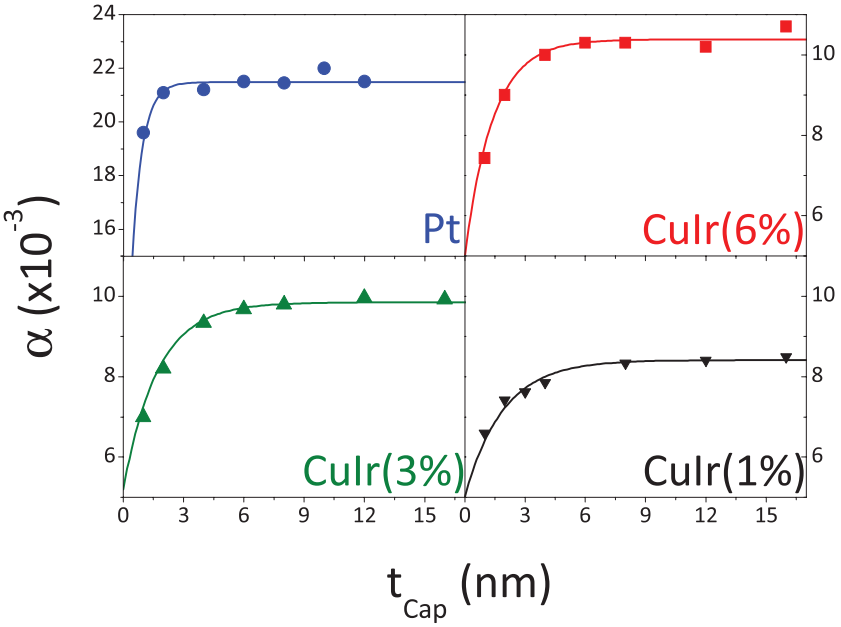

Figure 6. Damping parameter of 4 nm thick Py thin films capped with CuIr or Pt layers of thickness (t_{Cap}, where Cap = Pt, CuIr(6%), CuIr(3%) and CuIr(1%)). The solid lines refer to the fit using equation (7) and the parameters indicated in table 1.

contributions. In these conditions, the deduced damping from the frequency dependence of ΔH^{PP} using equation (6) is much closer to the Gilbert coefficient. This frequency dependence of ΔH^{PP} is plotted in figure 3(c) for Py films of various thicknesses capped with a 8 nm thick CuIr(6%) layer (figure 3(c)) and for 4 nm thick Py films capped with CuIr(6%) layer of a variable thickness (figure 4). For comparison, the frequency dependence of ΔH^{PP} for Py(3.5 nm) capped with a 5 nm thick Cu layer is also shown on figure 4 where a significant enhacement of the linewidth is observed as the CuIr(6%) thickness increases due to the larger spin pumping effect induced by CuIr(6%). The derived Gilbert coefficient using equation (6) increases with $1/(t_{Py} - t_d)$, as shown in figure 5(b). The increase of damping value with the FM inverse thickness using HM is attributed to spin pumping effect. By considering that the total damping is given by $\alpha = \alpha_{Py} + \alpha_{pump}$, where α_{Py} is the Gilbert damping of Py and α_{pump} is the damping introduced by the spin pumping effect due the metallic capping layer, the fitted data gives $\alpha_{Py} = 0.005$ (0.0066) for CuIr (Pt) capped films, which is slightly different from the usual intrinsic value of Py (≈0.006 [26]). The spin pumping contribution to the damping is given by [27, 28] $\alpha_{pump} = \frac{g\mu_B}{4\pi M_s(t_{Py} - t_d)} g_{eff}^{\downarrow\uparrow}$, where μ_B is the Bohr magneton and $t_{Py} - t_d$ is the Py effective thickness taking into account the magnetic dead layer thickness. $g_{eff}^{\downarrow\uparrow}$, which is the real part of the effective spin-mixing conductance, is the essential parameter to the spin pumping experiment. It accounts for the back flow of spin angular momentum from the nonmagnet back into the ferromagnet for both interfaces of the FM layer and refers to the efficiency of generating a spin current across the interface. From the fit of the experimental data the obtained values of $g_{eff}^{\downarrow\uparrow}$ are summarized in table 1 for all the samples studied here. This parameter increases with Ir doping rate. The obtained values for CuIr(6%) are of the same order than that measured for the Co/Ir systems (9.1 nm^{-2}) [29]. However, they are at least two times lower than that of Py/Pt systems, which is in good agreement with the previously obtained value by Du *et al* for $Ni_{81}Fe_{19}$/Pt (25 nm^{-2}) [30]. Furthermore, these values of $g_{eff}^{\downarrow\uparrow}$ for the different capping layers studied here remain largely higher than the obtained ones for YIG/Pt [31].

Increasing the spin current injection efficiency in FM/HM bilayer could be achieved by optimization of HM film thickness [32]. Indeed, with a large HM thickness most of the spin current generated in HM decays before returning to the FM interface due to the spin-flip scattering [9]. On the other hand, with small HM thickness, the net spin current is reduced due to the spin diffusion caused by the spin accumulation at HM surface. The HM thickness also affects the heat dissipation into the device electrodes and the rate of Joule heating [9]. Therefore, one can expect that there exists an optimal HM thickness for spin-injection into Py, determined mostly by the spin diffusion length. This spin diffusion length is thus an important parameter for describing SHE and ISHE. The dependence of the damping on HM capping layer thickness (t_{Cap}) can be described by [9]:

$$\alpha = \alpha_{Py} + \frac{g\mu_B}{4\pi M_s(t_{Py} - t_d)} g_{Cap}^{\downarrow\uparrow}\left(1 - e^{\frac{-2t_{Cap}}{\lambda_{Cap}}}\right) \qquad (7)$$

where λ_{Cap} is the spin diffusion length and $g_{Cap}^{\downarrow\uparrow}$ is the effective spin mixing conductance of the capping layer (Cap = Pt or CuIr). In our samples where, the buffer layer is SiO_2, the principle source of spin pumping is the capping layer and therefore, $g_{eff}^{\downarrow\uparrow}$ and $g_{Cap}^{\downarrow\uparrow}$ are identical. To determine λ_{Cap} and $g_{Cap}^{\downarrow\uparrow}$ for the Py/Pt and the Pt/CuIr interfaces, we deposited a series of samples with a constant Py layer thickness of 4 nm and a varied capping layer thickness t_{Cap}. Figure 6 shows the dependence of α versus t_{Cap} for both capping layers, where an exponential behavior is observed in good agreement with equation (7). By

fitting the experimental thickness dependence of the Gilbert damping with equation (7) and using the above mentioned values of α_{Py}, we determine λ_{Cap} and $g^{\downarrow\uparrow}_{Cap}$ as shown in table 1. The obtained values $g^{\downarrow\uparrow}_{Cap}$ are in a good agreement compared to those of $g^{\downarrow\uparrow}_{eff}$ found above. The small discrepancy between the obtained values of $g^{\downarrow\uparrow}_{Cap}$ and $g^{\downarrow\uparrow}_{eff}$ gives an idea about the error bars. The spin diffusion length increases with decreasing Ir doping rates. This is expected, since the primary spin-flip scattering events are scatterings on Ir impurities. The smallest value obtained for CuIr(6%) ($\lambda_{CuIr} = 2.8$ nm) is higher than that of Pt ($\lambda_{Pt} = 1.05$ nm) due to the higher SOC of the Pt. The obtained value of λ_{Pt} is in good agreement with previously obtained ones [33, 34].

5. Conclusion

Gilbert damping parameter has been measured in Py/Pt and Py/CuIr systems with varying Py and capping thicknesses using MS-FMR technique. We quantified the spin-pumping contribution to the enhanced damping of the system by taking the spin diffusion length of Pt and CuIr layers and the spin mixing conductance of the Py/Pt and Py/CuIr interfaces into account. We showed that the spin mixing conductance (spin diffusion length) decreases (increases) with decreasing Ir doping rates but remains considerably lower (higher) than that of Pt. Moreover, the perpendicular surface anisotropy constant present in the different samples capped by the various layers has been determined.

Acknowledgments

MG and CT acknowledge the financial support of the project SPINTRONIC: POS CCE ID. 574, code SMIS-CSNR 12467.

References

[1] Zutic I, Fabian J and Sarma S D 2004 *Rev. Mod. Phys.* **76** 323
[2] Jedema F J, Filip A T and van Wees B J 2001 *Nature* **410** 345
[3] Takahashi S and Maekawa S 2003 *Phys. Rev.* B **67** 052409
[4] Dyakonov M I and Perel V I 1971 *Phys. Lett.* A **35** 459
[5] Hirsch J E 1999 *Phys. Rev. Lett.* **83** 1834
[6] Zhang S 2000 *Phys. Rev. Lett.* **85** 393
[7] Valenzuela S O and Tinkham M 2006 *Nature* **442** 176–9
[8] Bosu S, Sakuraba Y, Uchida K, Saito K, Ota T, Saitoh E and Takanashi K 2011 *Phys. Rev.* B **83** 224401
[9] Shaw J M, Nembach H T and Silva T J 2012 *Phys. Rev.* B **85** 054412
[10] Heinrich B, Burrowes C, Montoya E, Kardasz B, Girt E, Song Y Y, Sun Y Y and Wu M Z 2011 *Phys. Rev. Lett.* **107** 066604
[11] Werake L K, Ruzicka B A and Zhao H 2011 *Phys. Rev. Lett.* **106** 107205
[12] Saitoh E, Ueda M, Miyajima H and Tatara G 2006 *Appl. Phys. Lett.* **88** 182509
[13] Costache M V, Sladkov M, Watts S M, van der Wal C H and van Wees B J 2006 *Phys. Rev. Lett.* **97** 216603
[14] Fert A, Friederich A and Hamzic A 1981 *J. Magn. Magn. Mater.* **24** 231
[15] Fert A and Levy P M 2011 *Phys. Rev. Lett.* **106** 157208
[16] Niimi Y, Morota M, Wei D H, Deranlot C, Basletic M, Hamzic A, Fert A and Otani Y 2011 *Phys. Rev. Lett.* **106** 126601
[17] Slonczewski J C 1999 *J. Magn. Magn. Mater.* **195** L261
[18] Sun J Z 2000 *Phys. Rev.* B **62** 570
[19] Koch R H, Katine J A and Sun J Z 2004 *Phys. Rev. Lett.* **92** 088302
[20] Belmeguenai M, Tuzcuoglu H, Gabor M S, Petrisor T Jr, Tiusan C, Berling D, Zighem F, Chauveau T, Ch S M and Moch P 2013 *Phys. Rev.* B **87** 184431
[21] Zakeri K *et al* 2007 *Phys. Rev.* B **76** 104416
[22] Arias R and Mills D L 1999 *Phys. Rev.* B **60** 7395
[23] Mills D L and Arias R 2006 *Physica* B **384** 147
[24] Arias R and Mills D L 2000 *J. Appl. Phys.* **87** 5455
[25] Shaw J M, Nembach H T, Silva T J and Boone C T 2013 *J. Appl. Phys.* **114** 243906
[26] Tserkovnyak Y, Brataas A and Bauer G E W 2002 *Phys. Rev. Lett.* **88** 117601
[27] Tserkovnyak Y, Brataas A and Halperin B I 2005 *Rev. Mod. Phys.* **77** 1375
[28] Jiao H J and Bauer G E W 2013 *Phys. Rev. Lett.* **110** 217602
[29] Toka M, Bunyaev S A, Kakazei G N, Schmool D S, Atkinson D and Hindmarch A T 2015 *Phys. Rev. Lett.* **115** 056601
[30] Obstbaum M, Härtinger M, Bauer H G, Meier T, Swientek F, Back C H and Woltersdorf G 2014 *Phys. Rev.* B **89** 060407
[31] Du C, Wang H, Yang F and Hammel P C 2014 *Phys. Rev. Appl.* **1** 044004
[32] Ulrichs H, Demidov V E, Demokritov S O, Lim W L, Melander J, Ebrahim-Zadeh N and Urazhdin S 2013 *Appl. Phys. Lett.* **102** 132402
[33] Zhang W, Vlaminck V, Pearson J E, Divan R, Bader S D and Hoffmann A 2013 *Appl. Phys. Lett.* **103** 242414
[34] Kondou K, Sukegawa H, Mitani S, Tsukagoshi K and Kasai S 2012 *Appl. Phys. Express* **5** 073002